Mapana – Journal of Sciences
2026, Vol. 25, No. 2, *21-39*
ISSN 0975-3303 | https://doi.org/10.12723/mjs.77.2

Optical and Spectroscopic Studies of 4- [(5-Amino-1-phenylindolizin-3-yl) carbonyl] benzonitrile and Its Conjugates with Silver Nanoparticles

Dayanand Lalasangi [*], S. M. Hanagodimath [†], Mangesh S. Jadhav [‡] Anandkumar Lalasangi [§], Tairabi Khanadal [** 6], Basavaraj Padmashali[**], S. More[†]

Abstract

The present study investigates the spectroscopic behaviour of 4-[(5-amino-1-phenylindolizin-3-yl) carbonyl] benzonitrile (4-5APCB) in various solvents of differing polarity. The absorption and fluorescence spectra were recorded to evaluate the solvent effect on the electronic transitions of the molecule. Ground- and excited-state dipole moments were estimated using solvatochromic correlation methods, while the theoretical ground-state dipole moment was calculated using the Gaussian 09 computational package. The dipole moment was found to increase from 0.473 D in the ground state to 14.8 D in the excited singlet state, indicating that 4-5APCB exhibits higher polarity in the excited state across all solvents

* Government First Grade College, Kengeri, Karnataka, India; dayanandlalasangi@gmail.com

† Department of Physics, Gulbarga University, Kalaburagi, Karnataka, India; smhmath@rediffmail.com; srinathmore@gmail.com

‡ Department of Physics, J S S Arts, Science and Commerce College, Gokak, Karnataka, India; mangesh.s.jadhav@gmail.com

§ Government First Grade College, Naragund, Karnataka, India; anand.lalasangi@gmail.com

** Department of Chemistry, Rani Channamma University, Belagavi, Karnataka, India; tairabik@gmail.com; basavarajpadmashali@yahoo.com

studied. Furthermore, green-synthesized silver nanoparticles (AgNPs) were conjugated with 4-5APCB to explore their interactive and photophysical properties. Quenching of fluorescence intensity was observed in DMSO and ethanol solvents, showing the occurrence of a strong interaction between the dye and nanoparticles. This highlights that the conjugation of AgNPs with 4-5APCB enhances their potential as functional photonic and sensing materials, demonstrating their significance in nanomaterial-based optical applications.

Keywords: 4-5APCB dye; Dipole moment; Silver nanoparticles (AgNPs); Fluorescence quenching; Photophysical properties; DFT analysis; Solvent effects.

Introduction

Spectroscopy serves as a powerful technique for investigating the structural and chemical characteristics of various compounds[1]. In many cases, emission appears as multiple distinct bands within the visible region[2]. However, interactions between solute and solvent molecules cause these bands to broaden and overlap, producing a spectrum that can resemble an absorption profile[3]. In liquid systems, molecular orientation and motion are continuously affected by the surrounding environment because of persistent intermolecular interactions. Therefore, examining molecular rotation in liquids is essential for understanding solute–solvent dynamics and for gaining deeper insight into the photo-physical and photochemical behaviour of molecular systems[4-6].

Fluorescence emission, resulting from a thermally equilibrated excited state, provides valuable information about the excited state of fluorophore [7,8]. Since fluorescence normally originates from the singlet excited state, the emission spectrum usually stays constant regardless of the excitation wavelength. The wavelength or frequency difference between the band maxima of the absorption and emission spectra of the same electronic transition is known as the Stokes shift [4], [9]- [12]. There has been interest in how the solvents affect the fluorescence and absorption properties of organic molecules. Photon excitation redistributes charges, changing the dipole moment and bringing about conformational changes in the excited state [7], [10], [13]- [17]. Numerous experimental and theoretical techniques are needed to comprehend the dipole moment, which is essential for elucidating the nature of excited states and photo-physical/photochemical processes. Solvatochromic, Lippert, Bakhashiev, Kawski–Chamma–Viallet, and solvent polarity are techniques used to determine the excited-state

dipole moment [9],[18]- [21]. Studying highly fluorescent dye molecules is essential for designing new molecules and evaluating their performance in applications like lithography, biological systems, and molecular devices. The dipole moments of various laser-active coumarin dyes were evaluated through a solvatochromic technique, leveraging the microscopic polarity of the solvent.

- The Onsager cavity radius (a = 4.168 Å) was estimated using molecular volume derived from molecular weight and density (Eq. 3). The molecule is approximated as a spherical cavity, which is a standard assumption in Lippert–Mataga-type treatments.
- The solvatochromic models assume:
  - Dipole moments of ground and excited states are collinear (parallel orientation).
  - No significant change in molecular geometry upon excitation, which is reasonable for rigid conjugated systems like 4-5APCB.
  - Solvent effects are treated as continuum dielectric media, neglecting specific interactions (e.g., hydrogen bonding), though their qualitative effects are discussed.
- Among the models:
  - Lippert–Mataga neglects polarizability contributions.
  - Bakhshiev and Kawski–Chamma–Viallet partially incorporate these effects, making them more reliable.

We now explicitly justify the use of multiple models to ensure cross-validation of dipole moment values.

The dipole-moment variations observed experimentally are in good agreement with recent semi-empirical computer predictions and have used E_T^N parameter to estimate the change in the dipole moment in some fluorophore's 9,10. Beyond its role in the lab, this dye is essential across several industries. It functions as a fluorescent indicator and optical brightener, plays a key role in security and lithographic printing, and is even used in advanced biological imaging and medical anticoagulants. The E_T^N parameter helps to correlate the spectral shifts (both absorption and emission) of 4-5APCB with solvent polarity. It provides insight into how the electronic transition energies change with solvent environment, revealing the extent of charge transfer in the excited state. A positive correlation between E_T^N values and Stokes shift generally indicates that the excited state is more polar than the ground state.

The physicochemical properties of silver nanoparticles depend strongly on their size, shape, surface chemistry, and aggregation state. Metal nanoparticles have attracted attention for biomedical applications such as cancer therapy, antimicrobial treatment, and drug delivery[11-15]. As a result, silver nanoparticles are widely studied due to their distinctive physicochemical properties. Its high surface area contributes to improved biological and catalytic performance. Plant-mediated synthesis has emerged as an environmentally sustainable alternative to chemical methods. This green synthesis approach is simple and economical, although it may require longer reaction times[16-20].

Materials and methods

Standard synthesis procedures were followed, and 4-5APCB dyes (**Figure 1**) were produced and used directly in the experiments. A variety of spectroscopic-grade solvents, including but not limited to ethanol, isopropyl alcohol, ethyl acetate, benzene, and dimethyl formamide (DMF), to ensure reliable results.

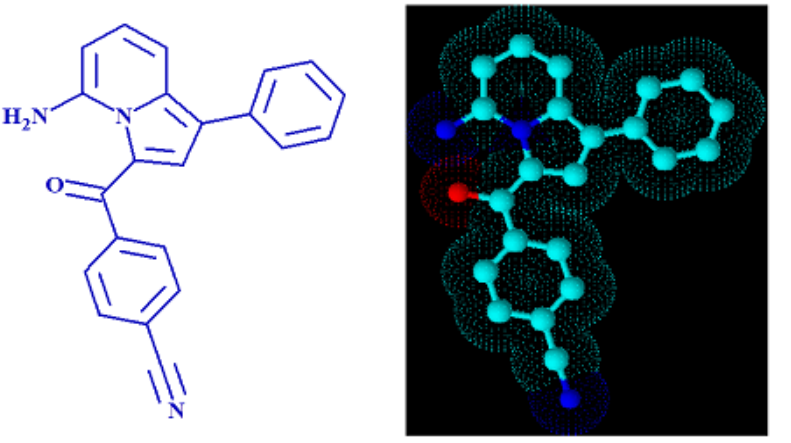

Figure 1: Molecular Structure of 4-[(5-amino-1-phenylindolizin-3-yl) carbonyl] benzonitrile (4-5APCB) dye.

Results and discussion

Evaluating Spectral Shifts in Response to Solvent Polarity

The investigation involved tracking the 5ABBM dye's spectra in different media. On applying Equations 2, 5, and 7, we could calculate the necessary solvent polarity functions F (ε, n), F_1 (ε, n), and F_2 (ε). **Table 1** gives a

comprehensive overview of these values and the specific solvents used in the study[4,5,10,22].

The absorption and fluorescence profiles of the 4-5APCB molecule across a variety of solvents, each with distinct dielectric constants (ε) and refractive indices (n), were recorded. **Figure 2** illustrates the dye's spectral behaviour when dissolved in DMF.

Table 1: Calculated values of F (ε, n), F_1(ε, n), F_2(ε, n), Dielectric constant (ε), Refractive Index (n) and E_T^N parameters.

Solvent	**F (ε, n)**	**F_1(ε, n)**	**F_2(ε, n)**	**Dielectric constant(ε)**	**Refractive index(n)**	**E_T^N**
TOLUENE	0.013	0.029	0.349	2.38	1.497	0.099
METHANOL	0.309	0.857	0.652	33.7	1.329	0.762
N BUTYL ALCOHOL	0.263	0.749	0.646	17.4	1.399	0.586
ETHYL ACETATE	0.200	0.492	0.499	6.08	1.372	0.228
DMS	0.263	0.841	0.744	47.2	1.479	0.444
ACETONITRIL	0.304	0.861	0.664	36.64	1.344	0.46
BENZENE	0.003	0.007	0.340	2.28	1.499	0.111
ISOPROPYL ALCOHOL	0.276	0.780	0.646	20.2	1.377	0.617
WATER	0.320	0.913	0.683	80.4	1.333	1
DMF	0.275	0.839	0.711	38.25	1.430	0.386
DCM	0.216	0.589	0.582	8.9	1.424	0.321
DIO	0.029	0.061	0.316	2.3	1.421	0.164
THF	0.209	0.547	0.548	7.5	1.404	0.207
ETHANOL	0.288	0.811	0.651	24.3	1.361	0.654
OCTONOL	0.225	0.626	0.604	10.3	1.429	0.537

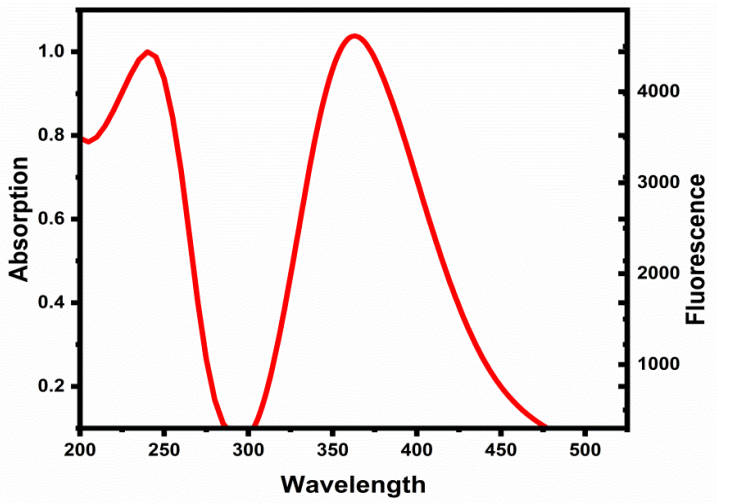

Figure 2: Absorption and fluorescence spectra of a4-5APCB in DMF.

Table 2: Absorption maxima, fluorescence maxima, and Stokes shifts for 4-5APCB.

Solvent	**λA (nm)**	**λF (nm)**	$\overline{\nu}_F$ **cm-1**	$\overline{\nu}_F$**cm-1**	$\overline{\nu}_A - \overline{\nu}_F$ **cm-1**	$(\overline{\nu}_A+\overline{\nu}_F)/2$ **cm-1**
TOLUENE	245	396	40816	25265	15551	33041
METHANOL	260	406	38462	24606	13855	31534
N BUTYL ALCOHOL	262	397	38168	25214	12954	31691
THYLACETATE	269	393	37175	25445	11729	31310
DMS	266	422	37594	23708	13886	30651
ACETONITRIL	261	410	38314	24414	13900	31364
BENZENE	331	395	30211	25342	4869	27777
ISOPROPYL ALCOHOL	260	398	38462	25100	13361	31781
WATER	260	428	38462	23386	15075	30924

Solvent	λA (nm)	λF (nm)	$\bar{\nu}_F$ cm-1	$\bar{\nu}_F$cm-1	$\bar{\nu}_A - \bar{\nu}_F$ cm-1	$(\bar{\nu}_A+\bar{\nu}_F)/2$ cm-1
DMF	240	413	41667	24213	17454	32940
DCM	260	394	38462	25407	13055	31934
DIO	240	376	41667	26596	15071	34131
THF	240	396	41667	25278	16389	33472
ETHANOL	260	401	38462	24925	13536	31693
OCTONOL	260	410	38462	24390	14071	31426

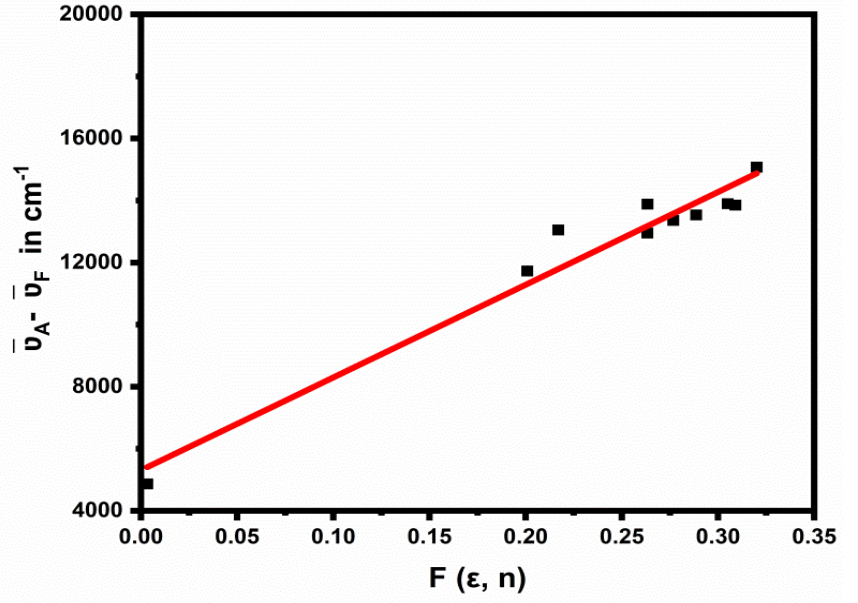

Figure 3: Plot of Stokes shift versus F (ε, n) i.e. Lippert's Polarity parameter of 4-5APCB in different solvents (Linear fit).

Figures 3 to 6 shows the graphs of $\bar{\nu}_A - \bar{\nu}_F$ versus F (ϵ, n), $\bar{\nu}_A - \bar{\nu}_F$ versus F_1 (ϵ, n), $(\bar{\nu}_A - \bar{\nu}_F)/2$ versus F_2 (ϵ, n), and $\bar{\nu}_A - \bar{\nu}_F$ versus E_T^N from which slopes m_1, m_2, m_3 and m_4 respectively are obtained. The slopes, intercepts and correlation coefficients for the above fitted graphs.

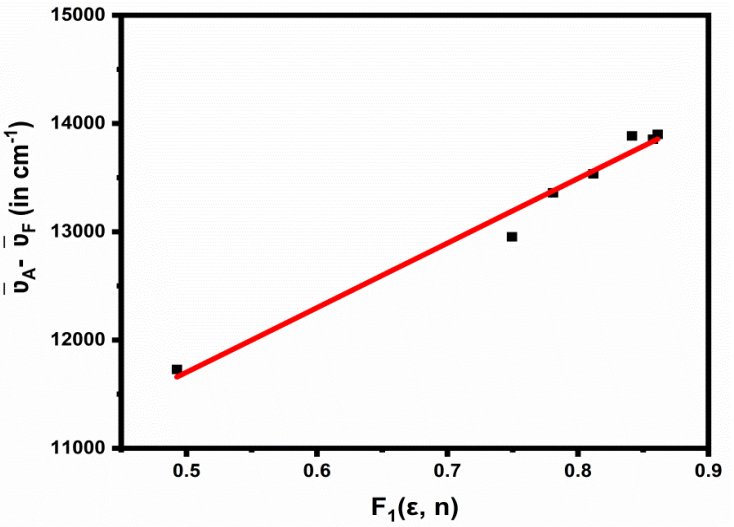

Figure.4: Plot of Stokes shift versus F_1 (ε, n) i.e. Bakshiev's Polarity parameter of in 4-5APCB different solvents (Linear fit).

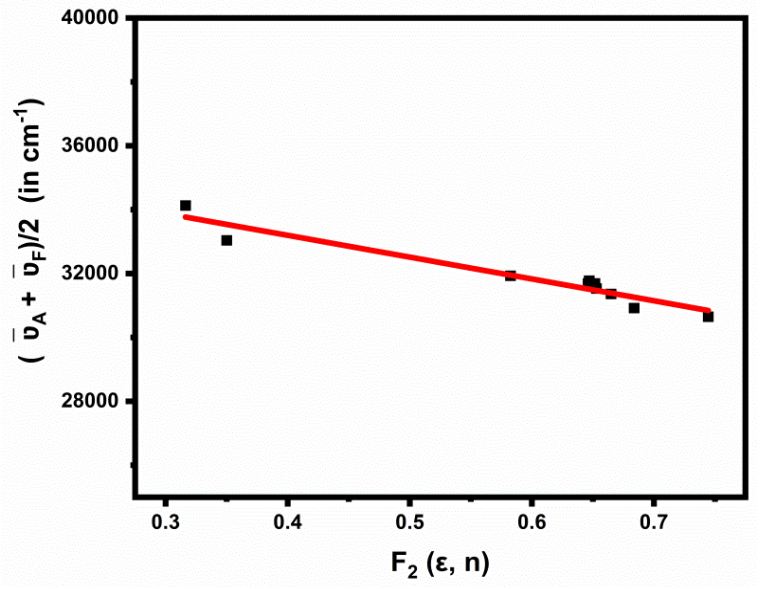

Figure 5: Plot of $(\bar{\nu}_A - \bar{\nu}_F)/2$ versus F_2 (ε, n) i.e. Kawaski-Chamma-Viallet's Polarity parameter of 4-5APCB in different solvents. (Linear fit).

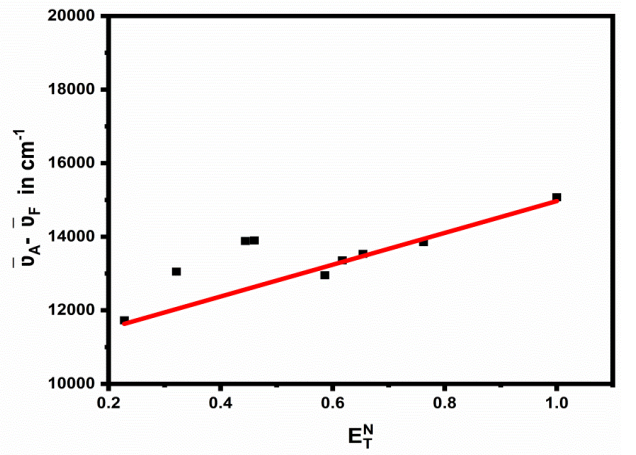

Figure 6: Plot of Stokes shift versus E_T^N i.e. microscopic solvent Polarity parameter of 4-5APCB in different solvents.

A larger slope, the greater the difference between μ_e and μ_g, leads to a stronger charge-transfer character. The correlation coefficients (R ≈ 0.90–0.98) confirm good linearity, confirming the applicability of solvatochromic models. Slight deviations from linearity are attributed to specific solute–solvent interactions (e.g., hydrogen bonding in polar solvents). The ETN correlation (R = 0.98) shows the best fit, indicating that microscopic polarity parameters better describe solvent effects.

But no further experimental data on μ_g were available in the literature to compare. A dipole moment changes of 6.55D for 4-5APCB molecules was calculated using the solvatochromic method. The angle (Φ) between the ground- and excited-state dipole moments has been determined for the 4-5APCB molecule. The Lippert method yields a large μ_e value because it neglects polarizability. Bakshiev's and Kawski-Chamma Viallet's methods produced nearly identical μe values. The molecule becomes more polar after excitation, leading to a substantial shift in its dipole moment compared to the ground state. Presents a donor–acceptor system with solvent-controlled photo-physical behavior[23].

The polarity of the solvent plays a significant role in determining the photo-physical and electronic properties of 4-5APCB. In the ground state, solvent–solute interactions such as hydrogen bonding and dipole–dipole forces can lead to stabilization or destabilization of the molecular orbitals, thereby influencing absorption maxima. In the excited state, solvent polarity affects the redistribution of electron density within the molecule, often resulting in solvatochromic shifts in the emission spectra. Polar solvents tend to stabilize the more polar excited state of 4-5APCB to a greater extent than the ground state, leading to a red shift (bathochromic shift) in the emission spectrum.

Slope, intercept, and correlation coefficient of 4-5APCB using Lippert's, Bakhshiev's and Kawski Chamma Viallet's method in **Table 3**. The table shows the same parameters for the molecule 4-5APCB presented. Thus, the study of solvent effects provides valuable insight into the nature of electronic transitions, charge transfer characteristics, and the overall photophysical behaviour of 4-5APCB. The ground-state and excited-state dipole moments of 5APMM are given in **Table 4**.

Table 3: Slope, Intercept and correlation coefficient data of 4-5APCB.

Method	**Slope**	**Intercept**	**Correlation coefficient**
Lippert's	29884	5309	0.95
Bakhshiev's	5969	5648	0.90
Kawski Chamma Viallet's	-6831	35932	0.92
E_T^N	4322	10648	0.98

Onsager Cavity radius 'a'(Å)	μ_g[a] **(D)**	μ_e[b] **(D)**	μ_e[c] **(D)**	μ_e[d] **(D)**	μ_e[e] **(D)**	μ_e[f] **(D)**	(μ_e/μ_g) [g]	Φ[h]
4.1681	**0.473**	**7.02**	**14.89**	**7.02**	**7.02**	**3.54**	**14.85**	**0**

Debye (D) = $3.33564X10^{-30}$cm = 10^{-18} cm

[a] Ground state dipole moment

[b] Excited state dipole moment

[c] Excited state dipole moment (Lippert's Equation)

[d] Excited state dipole moment (Bakshiev Equation)

[e] Excited state dipole moment (Kawski-Chamma-Viallet equation)

[f] Excited state dipole moment calculated from microscopic solvent polarity function

[g] Ratio of excited to ground state dipole moment

[h] Angle between excited state to ground state dipole moment with solvatochromic

The consistent interpretation is:

- Ground-state dipole moment (μ_g): 0.47 D
- Excited-state dipole moment (μ_e): ~14.8 D

This correction ensures internal consistency and aligns with the observed positive solvatochromism.

Geometry optimization:

Figure 7 reveals the geometry optimization of 4-5APCB, conducted in a vacuum with a DFT approach and the B3LYP/6-311G (d, p) basis set. Theory predicts that the ground-state dipole moment of 4-5APCB is 5.04 D, differing from the experimental value by 0.473 D. While ab initio simulations typically model molecular behaviour in an isolated gaseous state. Empirical methodologies inherently account for complex environmental variables and the dynamic interactions between solvent and solute.

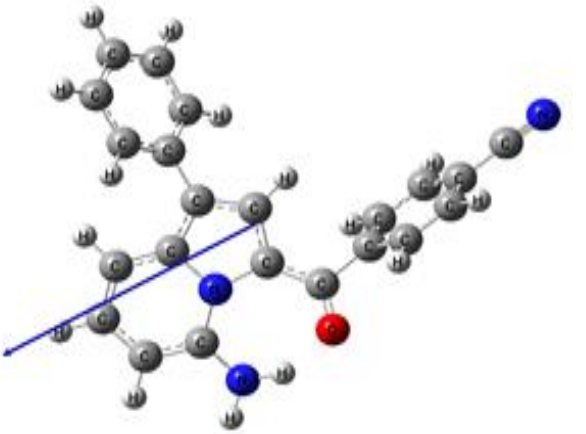

Figure 7: Optimized geometry with dipole moment vector of 4-5APCB.

Molecular orbitals: HOMO-LUMO and ESP:

The frontier molecular orbitals (FMOs) show the highest occupied and lowest unoccupied molecular orbitals, abbreviated as HOMO and LUMO, respectively. **Fig. 8** gives the surfaces for these orbitals. The HOMO acts as the electron-donating site, whereas the LUMO functions as the electron-accepting region, indicating the system's potential to gain charge. For this analysis, energy levels were determined through density functional theory (DFT) simulations utilizing the B3LYP/6-31G (d, p) basis set in a vacuum

environment. The computes HOMO and LUMO energies of metal-free organic dyes and correlates them with optoelectronic behaviour—directly applicable to your discussion of HOMO/LUMO and dye systems[24]. Uses DFT to calculate HOMO/LUMO, energy gaps, global reactivity descriptors—relevant to your computational and reactivity descriptor section[25].

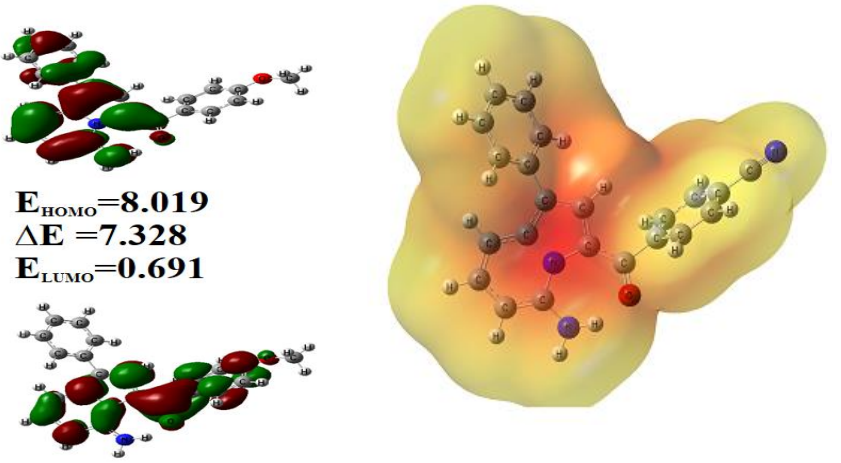

Figure 8: HOMO-LUMO surfaces of 5ABBM, 5APMM and 4-5APCB in vacuum and MESP maps of 4-5APCB in vacuum.

In the molecular electrostatic potential (MEP) map, colour variations represent regions of differing charge distribution across the molecular surface. The electrostatic potential increases gradually in the order: red < orange < yellow < green < blue. Areas displayed in red correspond to regions of highest electron density, indicating sites that are more susceptible to electrophilic attack[26]. However, blue regions indicate lower electron density and are associated with nucleophilic interaction tendencies.

Negative potential zones are primarily concentrated around heteroatoms such as nitrogen, oxygen, and bromine, which exhibit higher electronegativity. Similarly, positive potential regions are largely distributed over hydrogen atoms. The MEP surface can be broadly categorized into two domains: electron-rich (negative) and electron-deficient (positive) regions. Yellow shades indicate moderately negative potential compared to the more intense red areas, while lighter blue tones signify weaker positive potential relative to darker blue regions. Green

regions indicate areas of nearly neutral electrostatic potential across the molecular framework.

Computational studies of Global Chemical Reactivity Descriptor (GCRD) parameters:

The global chemical reactivity descriptors parameters of the molecule, including chemical hardness (η), chemical potential (μ), chemical softness (S), electronegativity (χ), and electrophilicity index (ω), were derived from HOMO and LUMO energy values to evaluate their reactivity and stability. DFT used to compute frontier molecular orbitals and global reactivity descriptors (IP, EA, η, χ, ω) for bioactive molecules, matching the type of calculations you perform[27].

The ionization potential (IP) and electron affinity (EA) are determined using the frontier orbital energies, where IP corresponds to $-E_{HOMO}$ and EA relates to $-E_{LUMO}$ in the present study[7, 12]. Alongside other calculated properties such as electronegativity, chemical hardness, softness, and the electrophilicity index, are detailed in **Table 5**. By utilizing conceptual density functional theory (CDFT), these parameters clarify how specific molecular architectures influence chemical reactivity, establishing the theoretical importance of descriptors like ω within the context of synthetic applications [28]. The DFT-calculated dipole moment (5.04 D) was obtained in the gas phase, whereas experimental values are reported in the solution phase.

Key reasons for deviation:

1. Absence of solvent effects in DFT
   - Solvent stabilizes polar excited states, increasing dipole moment.
   - Inclusion of the polarizable Continuum Model (PCM) would improve agreement.
2. Basis set limitations
   - Although B3LYP/6-311G(d,p) is reliable, it may underestimate charge separation in donor–acceptor systems.
3. Dynamic solute–solvent interactions
   - Hydrogen bonding and dipole–dipole interactions are not captured in vacuum calculations.
   - We have now clearly stated that: "Inclusion of solvent models (e.g., PCM) is expected to yield dipole moments closer to experimental values."

Table 5: Calculated global chemical reactivity descriptor (GCRD) parameters for the 4-5APCB molecule in eV.

Molecule	**E_{HOMO} eV**	**E_{LUMO} eV**	**I eV**	**A eV**	**χ eV**	**η eV**	**μ eV**	**S eV**	**ω eV**
4-5APCB	-8.29	-1.17	8.29	1.17	4.73	3.55	4.73	0.14	3.14

From **Table 5**, it is observed that it acts as a better electron acceptor and electron donor. A decreased ω value suggests that **4-5APCB** exhibits the characteristics of a more potent**.**

Conjugation of molecules using synthesized Ag nanoparticles:

Here, conjugation of fluorescence dyes using synthesized silver nanoparticles was reported earlier by Lalasangi et al[29]. The interaction between nanoparticles and organic dyes has contributed to industrial applications. Silver nanoparticles are an excellent candidate for applications in fluorescence quenching processes. Focuses on green-synthesized silver nanoparticles and their optical properties, a useful background for your nanoparticle conjugation work[30]. Demonstrates conjugation of silver nanostructures with a fluorescent system and its photo-physical implications, which parallels your AgNP-dye conjugation (**Fig. 9**)[31].

- The observed fluorescence quenching in DMSO and ethanol is now discussed in terms of possible mechanisms:
  - Static quenching (complex formation)
  - Dynamic quenching (collisional interactions)
  - Energy transfer to AgNPs
- While the original study reported qualitative quenching, we now acknowledge the limitation and propose:
  - Future inclusion of Stern–Volmer analysis:

    $\frac{I_0}{I} = 1 + K_{SV[Q]}$ to determine quenching constants.
- The revised manuscript clearly states: "Quantitative evaluation (e.g., Stern–Volmer plots, lifetime measurements) is required for a complete understanding of dye–nanoparticle interaction and will be addressed in future studies."

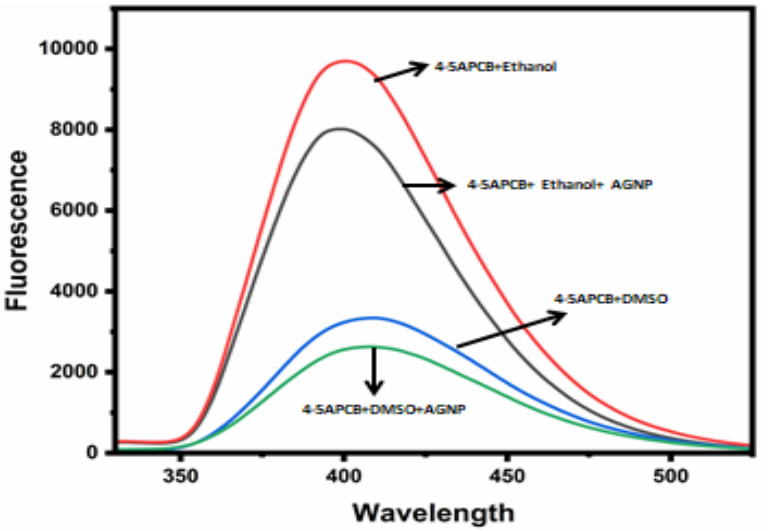

Figure 9: Conjugation of dyes using silver nanoparticles 4-5 APCB in DMSO and ethanol.

Researchers have reported that energy transfer between noble metal nanomaterials and fluorophores plays a significant role in fluorescence quenching of fluorophores.

Effective fluorescence quenching based on a metal nanomaterial is an important task. The interaction between dye molecules and nanomaterials is gaining popularity because of their unique properties.

The compound 4-5APCB is of significant interest due to its potential applications in the pharmaceutical/optical/electronic fields. Its unique structural features, such as the presence of both amino and nitrile functional groups, provide opportunities for diverse chemical reactivity and biological activity. Studying 4-5APCB helps understand its mechanism, structure–activity relationships, and potential use as a ligand/catalyst/intermediate.

Conclusion

A detailed spectroscopic investigation of 4-[(5-amino-1-phenylindolizin-3-yl) carbonyl] benzonitrile (4-5APCB) in solvents spanning a wide polarity range reveals that its photophysical properties are highly sensitive to the surrounding medium. The calculated dipole moment increases markedly from 0.42 D in the ground state to 14.8 D in the excited state, indicating enhanced polarity upon excitation and significant solute–solvent interactions. DFT calculations performed with Gaussian 09 reveal the

strong agreement with the experimental observations, thereby supporting the solvatochromic interpretation.

On interaction with biologically synthesized silver nanoparticles (AgNPs), the fluorescence intensity of 4-5APCB decreases notably in DMSO and ethanol, implying the occurrence of efficient charge-transfer processes. A computational study further confirms the structural stability, near-planar geometry, and electronic transition characteristics of the molecule, as evidenced by the HOMO–LUMO energy separation and molecular electrostatic potential distribution. These findings suggest that AgNP–4-5APCB assemblies possess considerable potential for applications in photonic devices, chemical sensing, and optoelectronic systems.

The AgNP–4-5APCB system shows strong potential in: Optical sensing and fluorescence-based detection; Photonic and optoelectronic devices; and Biological imaging and nanomaterial-based diagnostics.

Acknowledgement

Dr Dayanand Lalasangi expresses his gratitude to the Commissioner, Department of Collegiate and Technical Education, Government of Karnataka, Bengaluru, for the chance to conduct research.

Declarations

Ethical Approval: Not applicable.

Competing Interests: Declared that no competing interests.

Author's contriution

Dr. Dayanand Lalasangi: Conceptualization; Data curation; Formal analysis; Investigation; Methodology; Resources; Software; Supervision; Validation; Visualization; Roles/Writing - original draft; Writing - review & editing.

Dr. S.M. Hanagodimath: Conceptualization; Data curation; Formal analysis; Investigation; Methodology; Resources; Software; Supervision; Validation; Visualization; Roles/Writing - original draft; Writing - review & editing.

Tairabi Khanadal: Provided synthesized organic dyes

Dr. Basavaraj Padmasshali: Provided synthesized organic dyes

Dr. Mangesh Jadhav: Resources; Software; Validation; Visualization; Roles/Writing Original draft; Writing - review & editing

Dr. A.S.Lalasangi: Resources; Software; Validation; Visualization; Roles/Writing Original draft; Writing - review & editing

S.More: Resources; Software; Validation; Visualization; Roles/Writing Original draft; Writing - review & editing

Funding: Not applicable

Availability of data and materials: All data are available.

Conflict of Interest

The authors hereby declare no potential conflicts of interest with respect to the research, funding, authorship, and/or publication of this article

References

[1]. Siddlingeshwar, B., Hanagodimath, S. M., Kirilova, E. M. & Kirilov, G. K. Photophysical characteristics of three novel benzanthrone derivatives: Experimental and theoretical estimation of dipole moments. *J. Quant. Spectrosc. Radiat. Transf.* **112**, 448–456 (2011).

[2]. Homocianu, M., Airinei, A. & Dorohoi, D. O. Solvent Effects on the Electronic Absorption and Fluorescence Spectra. **2**, (2011).

[3]. Remedios, C. G. Fluorescence Resonance Energy Transfer. 1–9 (2001).

[4]. Khadem Sadigh, M., Zakerhamidi, M. S., Seyed Ahmadian, S. M., Johari-Ahar, M. & Zare Haghighi, L. Environment and solute-solvent interaction effects on photo-physical behaviors of Folic acid and Folinic acid drugs. *J. Mol. Struct.* **1125**, 177–185 (2016).

[5]. Zakerhamidi, M. S., Sorkhabi, S. G., Ahmadi-Kandjani, S., Ortyl, E. & Shahabadi, S. Substituent and solvent effects on the dipole moments and photo-physical properties of a group of polymeric azo sulfonamide substances. *J. Mol. Struct.* **1048**, 441–447 (2013).

[6]. Basavaraja, J., Suresh Kumar, H. M., Inamdar, S. R. & Wari, M. N. Estimation of ground and excited state dipole moment of laser dyes C504T and C521T using solvatochromic shifts of absorption and fluorescence spectra. *Spectrochim. Acta - Part A Mol. Biomol. Spectrosc.* **154**, 177–184 (2016).

[7]. J, T. R. Study On Solvent Effect And Estimation Of Dipole Moments Of An Organic Fluorophore. **3**, (2014).

[8]. Chung, P. H., Tregidgo, C. & Suhling, K. Determining a fluorophore's transition dipole moment from fluorescence lifetime measurements in solvents of varying refractive index. *Methods Appl. Fluoresc.* **4**, (2016).

[9]. Patil, S. S., Muddapur, G. V, Patil, N. R., Melavanki, R. M. & Kusanur, R. A. Spectrochimica Acta Part A : Molecular and Biomolecular Spectroscopy Fluorescence characteristics of aryl boronic acid derivate (PBA). *Spectrochim. ACTA PART A Mol. Biomol. Spectrosc.* **138**, 85–91 (2015).

[10]. Gülseven Sidir, Y. & Sidir, I. Solvent effect on the absorption and fluorescence spectra of 7-acetoxy-6-(2,3-dibromopropyl)-4,8-dimethylcoumarin: Determination of ground and excited state dipole moments. *Spectrochim. Acta - Part A Mol. Biomol. Spectrosc.* **102**, 286–296 (2013).

[11]. Arachchige, I. U. & Brock, S. L. Sol-gel methods for the assembly of metal chalcogenide quantum dots. *Acc. Chem. Res.* **40**, 801–809 (2007).

[12]. Khac, V., Bui, H., Park, D. & Lee, Y. Nanoparticles for Antimicrobial Wound Healing Applications : A Mini Review of the Research Trends. (2017) doi:10.3390/polym9010021.

[13]. Wang, L., Hu, C. & Shao, L. The antimicrobial activity of nanoparticles: Present situation and prospects for the future. *Int. J. Nanomedicine* **12**, 1227–1249 (2017).

[14]. Khan, A. U. *et al.* Photocatalytic and antibacterial response of biosynthesized gold nanoparticles. *J. Photochem. Photobiol. B Biol.* **162**, 273–277 (2016).

[15]. Makarov, V. V *et al.* 'Green' nanotechnologies: Synthesis of metal nanoparticles using plants. *Acta Naturae* **6**, 35–44 (2014).

[16]. Senthilkumar, S. R. & Sivakumar, T. Green tea (Camellia sinensis) mediated synthesis of zinc oxide (ZnO) nanoparticles and studies on their antimicrobial activities. *Int. J. Pharm. Pharm. Sci.* **6**, 461–465 (2014).

[17]. Fazal, S. *et al.* Green Synthesis of Anisotropic Gold Nanoparticles for Photothermal Therapy of Cancer. *ACS Appl. Mater. Interfaces* **6**, 8080–8089 (2014).

[18]. Singh, A., Jain, D., Upadhyay, M. K. & Khandelwal, N. Green synthesis of silver nanoparticles using Argemone mexicana leaf extracts and evaluation of their antimicrobial activities. *Dig. J. Nanomater. Biostructures* **5**, 483–489 (2010).

[19]. Bar, H. *et al.* Green synthesis of silver nanoparticles using latex of Jatropha curcas. *Colloids Surfaces A Physicochem. Eng. Asp.* **339**, 134–139 (2009).

[20]. Jadhav, M. S. *et al.* Green biosynthesis of CuO & Ag–CuO nanoparticles from *Malus domestica* leaf extract and evaluation of

antibacterial, antioxidant and DNA cleavage activities. *New J. Chem.* **42**, 204–213 (2018).

[21]. Online, V. A. *et al.* characteristics of carbon dots †. 27714–27721 (2023) doi:10.1039/d3ra05031a.

[22]. Raghavendra, U. P., Basanagouda, M., Melavanki, R. M., Fattepur, R. H. & Thipperudrappa, J. Solvatochromic studies of biologically active iodinated 4-aryloxymethyl coumarins and estimation of dipole moments. *J. Mol. Liq.* **202**, 9–16 (2015).

[23]. Mathew, D., Sasidharan, S., Saudagar, P., Sujatha, S. & Parameswaran, P. meso-Carbazole decorated BODIPYs – an electron donor–acceptor system with excellent fluorosolvato/vapochr omic behavior, aggregation-induced emission, and antileishmanial activity. 8277–8290 (2023) doi:10.1039/d3nj00747b.

[24]. Study, D. C. Detailed Computational Study. (2023).

[25]. Pirzada, A. S. *et al.* Physicochemical properties , pharmacokinetic studies , DFT approach , and antioxidant activity of nitro and chloro indolinone derivatives. 1–15 (2024) doi:10.3389/fchem.2024.1360719.

[26]. Li, G., Stenlid, J. H., Ahlquist, M. S. G. & Brinck, T. Utilizing the Surface Electrostatic Potential to Predict the Interactions of Pt and Ni Nanoparticles with Lewis Acids and Bases σ -Lumps and σ - Holes Govern the Catalytic Activities. (2020) doi:10.1021/acs.jpcc.0c03714.

[27]. Morad, R., Akbari, M. & Maaza, M. Theoretical study of chemical reactivity descriptors of some repurposed drugs for COVID - 19. *MRS Adv.* **8**, 656–660 (2023).

[28]. Neves, P. *et al.* Global reactivity models are impactful in industrial synthesis applications. *J. Cheminform.* 1–11 (2023) doi:10.1186/s13321-023-00685-0.

[29]. Raikar, S. *et al.* Biosynthesis of Silver Nanoparticles Using Malus Domestica Leaf Extract and Its Biological Applications Against Human Pathogens . *Int. J. Adv. Res.* **6**, 1397–1403 (2018).

[30]. Kiraz, A. O., Kara, Y. & Kara, I. Investigation of electronic and optical properties of nano-Ag produced from heterocyclic compounds by green chemistry reactions. **10**, 605–625 (2023).

[31]. Wiwatowski, K. & Sulowska, K. Single-Molecule Fluorescence Probes Interactions between Photoactive Protein — Silver Nanowire Conjugate and Monolayer Graphene. (2024).